Jour. Fac. Sci., Hokkaido Univ., Ser. VII (Geophysics), Vol. 10, No. 2, 165-187, 1997.

# Internal Wave Rolls Observed with the TSP, and their Contribution to Turbulent Energy Transfer

**Yoshiro Kaya, Shoshiro Minobe and Seiichi Kanari**

*Division of Earth and Planetary Sciences, Graduate School of Science, Hokkaido University, Sapporo 060, Japan*

( Received November 31, 1996) )

**Abstract**

In order to investigate the role of wave breaking in mixing processes, we observe finestructures of temperature in a coastal region, by using a towed thermister chain, which referred to as Towed temperature Structure Profiler (TSP). Internal wave rolls with a wave length of about 15 m, which may be caused by the K-H instability, were captured by the TSP. The temperature field obtained by the TSP enable us to analyze turbulent processes due to internal wave breaking. Spatial scales of mixing patches associated with the internal wave rolls are estimated as about 300 m in horizontal and 2-3 m in vertical by examining the spatial distribution of wave number spectra. The radiative loss of energy from the mixing patch by internal waves are also estimated. An importance of 'pressure-velocity correlation divergence' term in the equation of turbulent kinetic energy budget in the coastal region was discussed.

## 1. Introduction

The ambiguity of diapycnal mixing coefficients is a major source of the uncertainty in the results of general circulation models (GCMs). In the vertical mixings in both the ocean interior and coastal regions, internal wave breaking due to wave instability are expected to play a crucial role. Most of studies have focused attentions on two wave instabilities: One is shear instability, which occurs when the vertical shear becomes large enough to overcome the opposing torque of stratification (Richardson, 1920; Miles, 1961). The other is buoyancy instability, which occurred when the wave fluctuations becomes large enough to advect heavy water over light water, producing unstable density gradients (Orlansky and Bryan, 1969; Thorpe, 1978). The shear instability is considered to be mainly caused by composition of waves in continuos spectrum in the ocean interior (Garret and Munk, 1979; Desaubies and Smith, 1982). At

the boundary region such as ocean bottom or near-shore, both the wave reflection from the slopes with critical angles (Eriksen, 1985) and the scattering of internal waves at the rough bottom topography (Müller and Xu, 1992) result in energy transfer from lower to higher wavenumber in which the waves reach to break. Therefore, for a better understanding for ocean mixing, we must study both the dynamical and kinematical balance of internal wave field. The mixing due to the wave breaking occurred in thin patch-like regions, which are called as mixing patches. So far, quantitative measurements of dissipation on the space and time scales of mixing patches are important to understand the dynamical chain of the internal-wave generation, redistribution, and decay. The validity of the diapycnal fluxes employed in large-scale models can be examined by these observations (Gregg, 1987).

Recent progress of observational techniques provided the information of the dependence of the oceanic structures to the wavelength in a range of 100 m to 1 cm (Gregg 1977, Gargett 1981). A distinctive feature of their spectrum is the 'rolloff' of a order of 10 m in vertical scale. The vertical scales smaller than the roll off scale (roughly 1 m to 10 m) are called as fine-scale, and the fluctuations of these scales are called as finestructures. Through the fine-scale, internal waves transfer energy to dissipation scales, which is smaller than 1 m (e.g., Munk, 1981 ; Garrett, 1979). In this energy transfer, internal wave breaking play an important role. Spectra in finestructures of both temperature gradients and vertical shear exhibit slopes of $-1$. Usually, finestructures are regarded as combinations of structures produced reversibly by internal wave strain and irreversibly by mixing (Desaubies and Gregg, 1981).

There are several experimental studies on the internal wave breaking, and most of those are laboratory experiments (e.g., Thorpe, 1973 ; Koop and Browand, 1979). The evolution of shear instability is seldom observed in the real ocean, except the pioneering work by Woods (1968) who observed evidence of the wave breaking by photographs.

A towed thermister chain, is a relatively new observation tool. This apparatus enable us to monitor temperature fields with a high resolution in vertical and time. The temporal temperature change observed by the towed chain can be interpreted as a horizontal change, when the propagation speed of the information in observed phenomena is one-order smaller than the tow speed. As a consequence, the towed thermister chain provides the quasi snap-shot with high vertical and horizontal resolutions, allowing us to examine the existence of the wave breaking. Towed thermister chain have the other advantage to the photograph observation. The chain observe the temperature with high accu-

racy, and hence one can estimate quantitative characteristics of the wave fields, by using, for example, spectrum analysis. Such analysis is not possible based on photograph observation. The purpose of the present paper, therefore, to observe the temperature field by towed thermister chain under the physical environments that one can expect the existence of the wave breaking. Hereafter the towed thermister chain system is referred to as Towed temperature Structure Profiler (TSP).

This paper is organized as follows: In section 2, the TSP that we developed is described. In section 3, first, the property of the observed internal wave rolls and the required condition for the wave instability are examined. Second, the spectrum analysis is presented and the spatial scales of mixing patches are estimated. Finally the relative importance of 'divergence of pressure-velocity correlation' term in the turbulent kinetic energy equation is evaluated. Summary and conclusion are given in section 4.

## 2. Instruments and observational backgrounds

### *2.1 Towed temperature Structure Profiler*

The first Towed temperature Structure Profiler was developed by LaFond (1963). This was a huge system, which included a drum, a hoist, and a link. Hence, an exclusive ship of US Navy was needed to tow the chain system. After the Lafond-type chain system, a higher performance systems was proposed by Mesecar and Evans (1977). However, it was still a heavy system, and cannot be used easily.

Recent developments of electronic devices afford us to make a smart system. With some improvements on switching circuits, and the harness, we developed a new towed temperature structure profiling system (hereafter we referred this system as TSP). This system is an array of 18 temperature sensors with 0.5 m intervals. The depth is monitored at the end of the system.

Each sensor is scanned with switching signals in every 0.3 sec. Thus, for a towing speed of 2.0 $ms^{-1}$, the resolution of the temperature structure in horizontal is about 0.6 m. As shown later, the highest phase speed of internal waves is estimated as the order of 0.1 $ms^{-1}$ for the present observation area. This speed is smaller by one order than the towing speed, indicating that the TSP can observe a snap shot of the temperature structure associated with variations of the internal waves. The vertical scale of 0.5 m is believed to divide fine-scale and micro-scale. Thus the TSP can well resolve-the finestructures. More technical detail of the TSP can be found in Kanari et al. (1996).

### 2.2 *Towing Observations*

A TSP-test cruise was carried out on November 21, 1993 at the site off the west coast of Awaji. The TSP with 18 temperature sensors was towed along the line AB shown in Fig. 1. Figure 2 shows the schematic plan of the TSP towing. For a typical towing speed of 2.0 $ms^{-1}$, tow depth was kept almost the same level of 14.6 m. The depth of the first sensor was 8.0 m, and the vertical distances between two sensors were 0.38 m in average.

In order to avoid that analyses are affected by the depth change of the sensors, we use the data that observed approximately at uniform depths. For this purpose, variations of the depth was examined. For each interval that has the 512 data, the mean depths were specified. This data number of 512 is chosen because it is suitable for the spectra analyses described in section 3. If a datum in a interval contains deviations over 0.3 m from the mean depth, this interval is not used for further analyses. Figure 3(a) exhibits the data whose temperature changes are not affected by the changes of the sensor depth (Fig. 3(b)), and the data are used in the later analyses. Because the ship speed was kept at 2.0 $ms^{-1}$, 5 minutes in Fig. 3 corresponds to the horizontal distance of 600 m. As described in section 3.1, we observed internal wave rolls at the left side of Fig. 3(a).

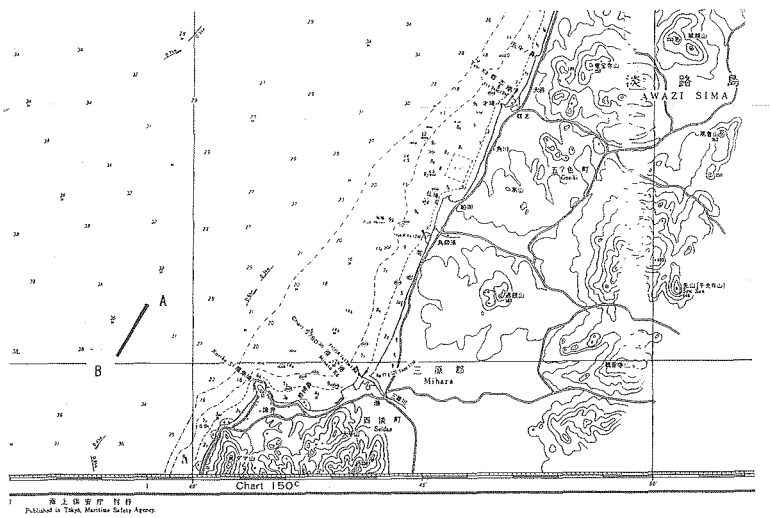


Fig. 1. Map of the observation location in Dec. 21, 1993. The TSP was towed from site A to site B, in the direction of south west. The distance between A and B is about 3 km.

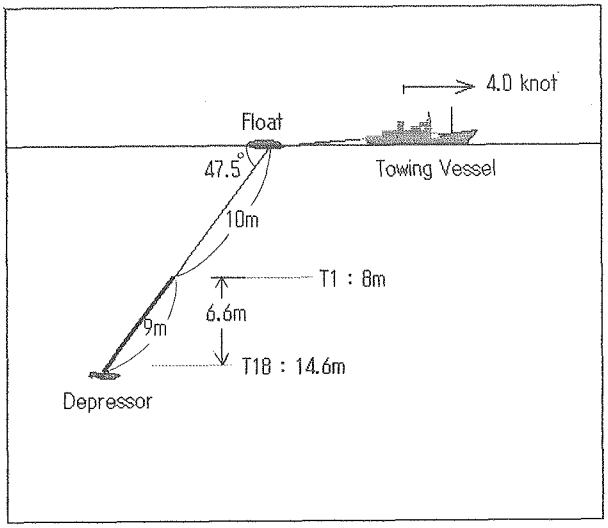


Fig. 2. Schematic view of TSP towing. The average towing speed is 2.0 $ms^{-1}$, with the depth of the deepest sensor at 14.6 m.

Vertical temperature and salinity profiles was observed at the site A. The T-S relation proved by the CTD profiling enable us to detect the Thorpe scale (see section 3.3). Both temperature (Fig. 4(a)) and salinity (Fig. 4(b)) are constant from surface to about 12 m depth as shown in Fig. 4. Similarly, there exists a bottom mixed layer for deeper than about 22 m. For the depth from 12 m to 22 m, the stratification is weakly stable. However, T-S relation is not so simple. A temperature inversion compensated by salinity is seen in 12 m to 22 m (Fig. 4(c)). The internal wave speed is estimated as the order of 0.1 $ms^{-1}$, from the density difference of 0.2 kg $m^{-3}$ between the upper and lower layers with the bottom depth of ~30 m. As mentioned above, this speed of the internal wave is small enough so that the TSP observes a snap shot of the wave field.

The velocity distribution of barotropic tidal flow at the time of towing, is shown in Fig. 5. The tidal streams correspond to the phase of 'Time of Turn of Tidal Streams to West' at the *Akashi* strait. The direction of the tidal flow at the site was along shore, toward the northeast. The amplitude of the tidal flow ranges from 0.1 kt to 0.5 kt.

## 3. Internal wave rolls

The observation with the TSP revealed the final stage of wave breaking in

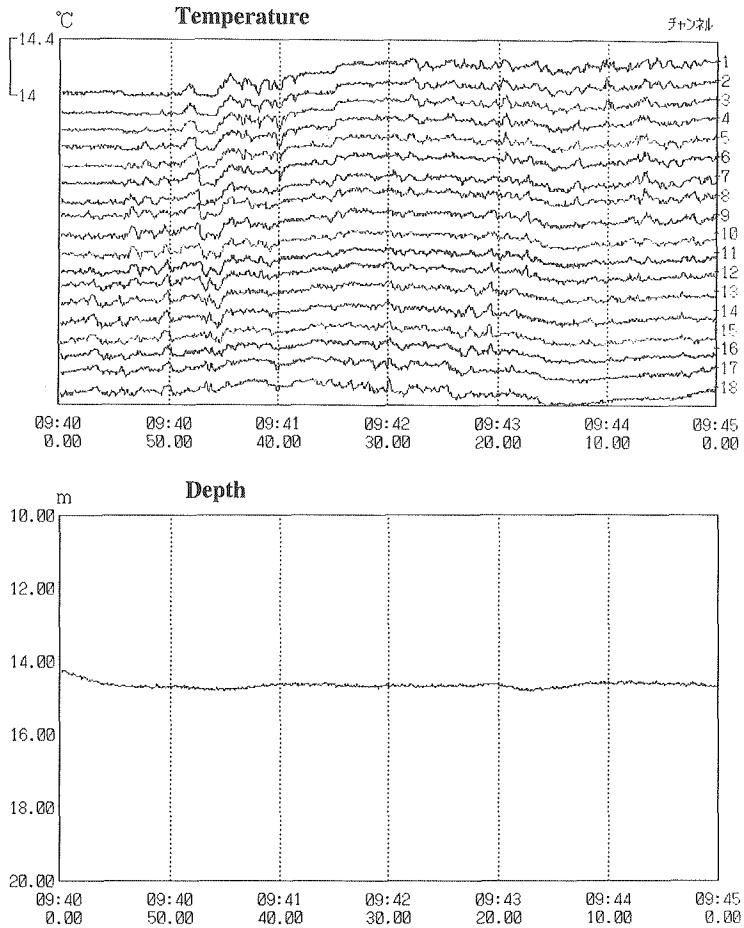


Fig. 3. (a) Temperature time-series observed respective sensors for the data that are not affected by the depth change, and (b) corresponding time-series of the depth at the deepest, eighteenth sensor. The deviation from the mean depth is very small for this time span, from 9 : 40 to 9 : 45. The scale of temperature variation, 14.0-14.4°C is indicated. Digits at right end denote the channel number of each sensor. The temperature between 09 : 40 : 20 and 09 : 40 : 50 is also shown in Fig. 6.

the real ocean. In section 3.1, the property of internal wave rolls observed with the TSP is described with some consideration about the required condition for the K-H instability. In section 3.2, temperature spectra obtained from the TSP data are examined. The spatial scale of mixing patches are also discussed with the wavenumber dependence of the spectra in the inertial subrange. In section

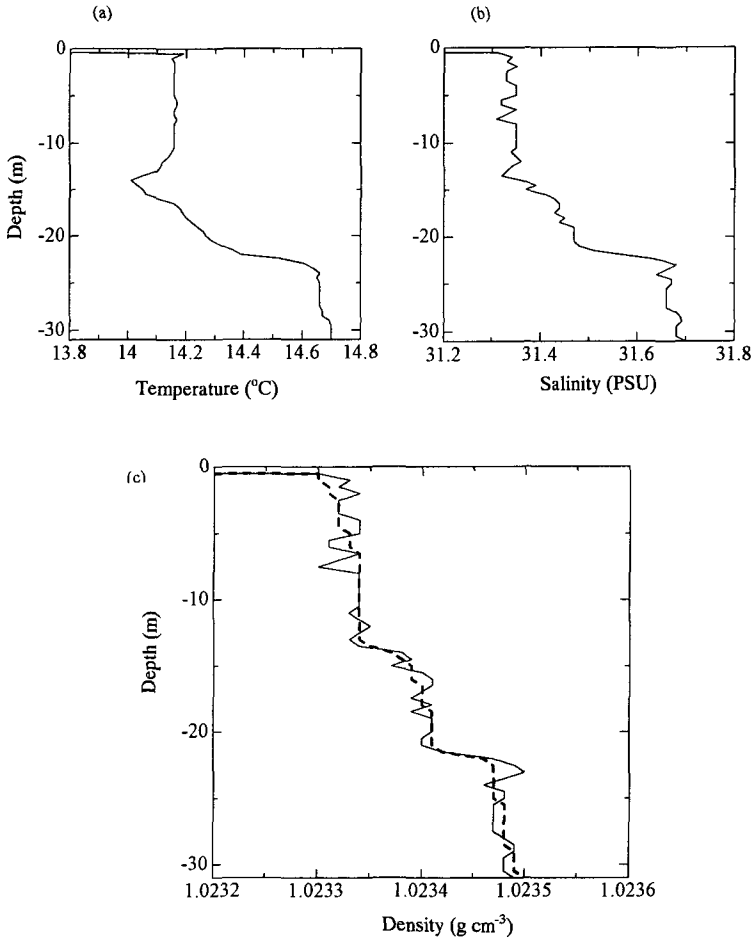


Fig. 4. Vertical profiles of (a) temperature, (b) salinity and density (c) observed with the CTD at site. The dashed line in (c) exhibits the Thorpe-ordered density profile.

3.3, the radiative energy loss from the patch boundary is considered. In the case where the mixing region exists in stratified shear fluid, the relative importance of the 'divergence of pressure-velocity correlation' is emphasized.

### *3.1 Observed internal wave rolls*

A temperature section that exhibits distinctive wave rolls is displayed in Fig. 6. The temperature structures are not affected by the change of the sensor

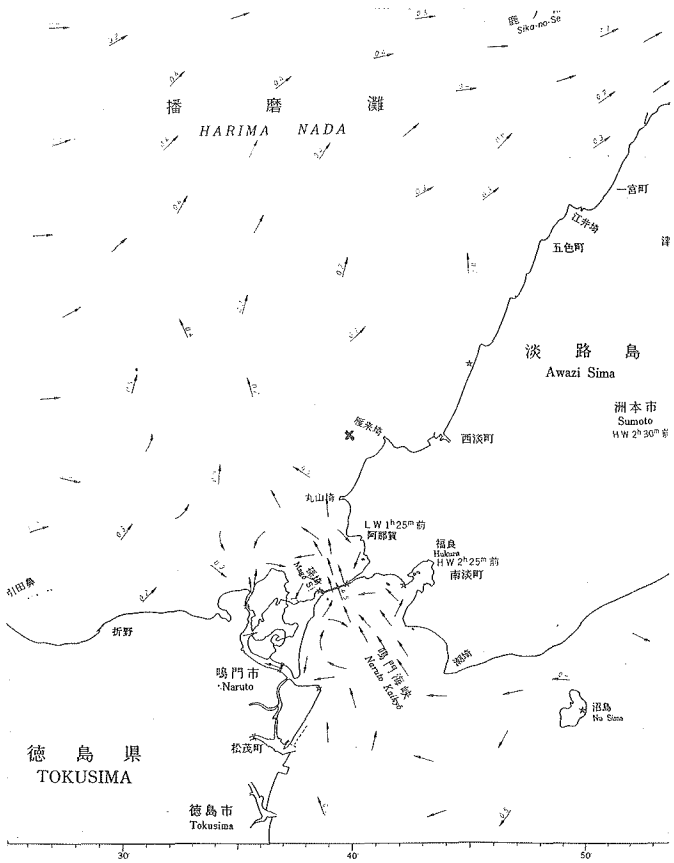


Fig. 5. Tidal flow chart at the observation time. Barotropic tidal flow from *Naruto straight* rises to 5.5 kt in the direction of north at this time.

depth as mentioned above. Figure 6 shows a train of four similar wavelets, which have narrow troughs and wide crests in the depth range of 9-13 m. Judging from Fig. 6, the horizontal wavelength of each wavelet is about 15 m, and its maximum height is about 2 m. Upper part of each wavelet obviously rolls in the same sense (North-East direction). At the time of towing, the direction of mean flow is presumably northeastward, and is along the shore. Rolling in the direction of the mean flow, and the regular alignment of these rolls are the characteristic properties of K-H billows. The observed 15 m wavelength, and waveheight of 2 m means the wave slope of 0.41. According to Thorpe (1978), internal waves are unstable if their slope exceeds 0.34 even in the

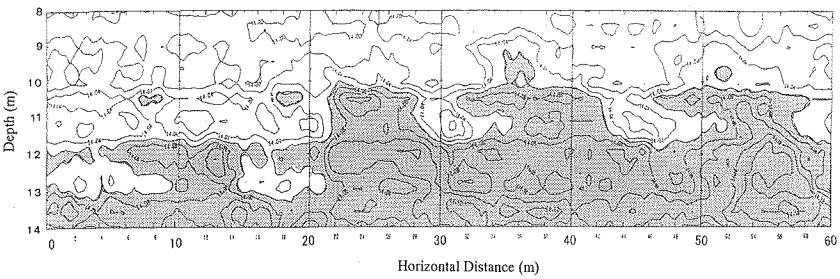


Fig. 6. Temperature section corresponding the time interval from 09 : 40 : 20 to 09 : 40 : 50 in Fig. 3. Hatched areas indicate the temperature warmer than 14.06°C. Four internal wave rolls are distinctively seen. Four wavelets are rolling in the same sense around the crests of longer wave length. Each wavelets has horizontal wavelength of about 15 m, and waveheight of about 2 m. The direction of rolling is in the direction of background flow i.e., north-east. This is consistent with the hypothesis that these structures are associated with the final stage of wave instability.

absence of ambient shear. Therefore, the observed internal waves are the most likely to be gravitationally unstable and break even if without ambient shear.

The above examination of the wave slope has indicated that the observed waves are expected to be in under breaking. For the present data, we could not take additional data to specify what process is responsible for the wave growth to the waves with the rather steep slope, however, we will speculate that the source of the wave growth is due to shear instability. According to Hazel (1972), assuming that waves with the 15 m wavelength are unstable due to the shear, a required velocity difference (maximum velocity minus minimum velocity) is only about 0.7 $ms^{-1}$. A shear of this order was quite possible, since the velocity of the barotropic tidal flow implied from the tidal charts was in the range from 0.05 $ms^{-1}$ to 0.25 $ms^{-1}$. As a consequence, the internal waves are likely to grow due to the instability associated with the vertical shear owing to the tidal flow, and the TSP has captured an instant of the grown-up waves just breaking.

### *3.2 Structure of temperature spectra*

Although wave rolls are a distinctive signal of the wave breaking, the rolls must be collapsed in short time. Therefore, even in some of the regions where the wave rolls are not detected as a snap-shot observed by the TSP, active wave breaking probably occurred. Such regions where wave breaking already took place could be expected to have patch-like structure of active mixing with a thin

vertical extent and much wider horizontal scale (e.g., Marmorino and Trump, 1992). Therefore, in order to distinguish whole spatial distribution of the mixing due to the wave breaking, we examine the existence of active mixing patches, using the spectrum structure in the temperature field.

The mixing due to the internal wave breaking is a process that transfers the wave energy with a vertical scale larger than 10 m into a scale smaller than 1 m. When the energy transfer from the larger scale occurs, the spectrum slope has the vertical wavenumber dependence of $k^{-5/3}$ (Kolmogoroff, 1941), and the motion in this small scale is identified as the turbulence of inertial subrange. In the inertial subrange, the motion is expected to be fairly isotropic. Thus, the

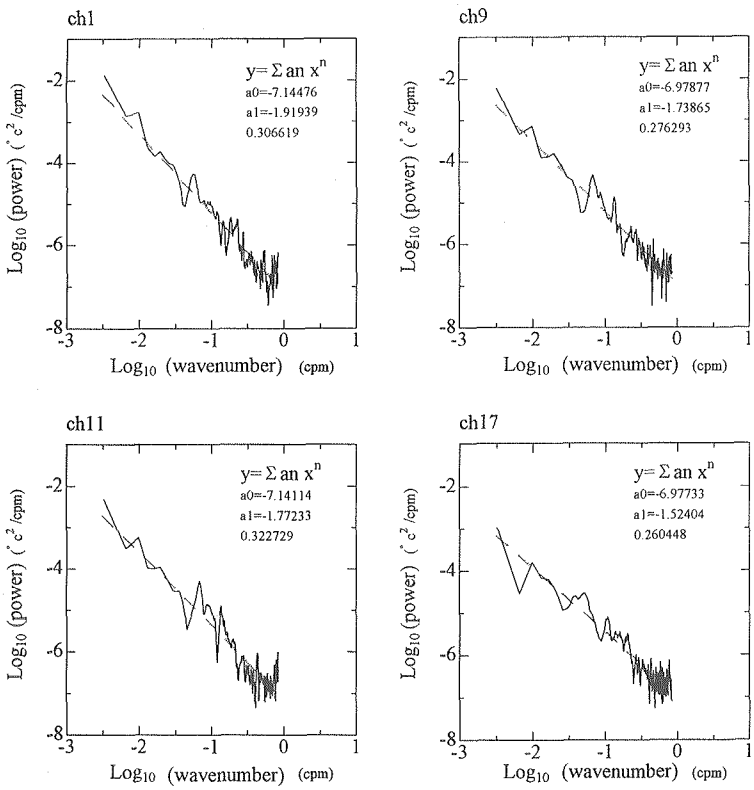


Fig. 7. Temperature spectra for horizontal wavenumber at four depth levels. The spectra are calculated for the horizontal span of 300 m including the roll like features. The digits next to 'ch' denote the channel numbers of the sensors. Spectra from ch 9 and ch 11 have slopes of approximately −1.67, which is the characteristic slope in intertial subrange.

vertical wavenumber dependence of $k^{-5/3}$ can be applied to the horizontal wavenumber spectrum.

Figure 7 shows the temperature fluctuation spectra from the data area where internal wave rolls were observed. They span the scale from about 1 m to 300 m. For larger horizontal scale than 300 m, spectra are affected by horizontal temperature gradients of large scale. The thin broken lines are of least squares fittings (first order), and the digits after the "al=" denote the regressive coefficients. For the spectrum calculation, a cosine taper applied to the first and last 10% of the time series, and the raw spectra were smoothed in wavenumber space. As seen in Fig. 7, the depth at where the breaker observed (sensor of 9th, and 11th, correspond to about 12 m depth), the wavenumber dependence of spectra has a slope of nearly $-5/3=-1.67$. Nevertheless, outside this region, such relation is not observed. Hence, we regard the $-5/3$ Spectrum slope as an evidence of the active turbulence in the inertial subrange.

In order to determine the spatial scale of mixing patches, we have to know the wavenumber dependence at each place. For this space-wavenumber analysis, we applied a dynamic spectrum method. A spectrum is calculated for a data segment of 512 data points, and the window of the data segment is moved to yield the horizontal distribution of the spectrum at every sensor depth. Then we obtain the contour map of the spectral slopes as shown in Fig. 8(a). The left end of the contour map corresponds to the location where the internal wave rolls were observed. As shown in Fig. 8(b), the temperature structure similar to the temperature profile of CTD was seen only in the left part of the contour map. In a wider area, there exists a stable thermocline, while the CTD data and the data of the very left part of Fig. 8b contain temperature inversion layers. In other word, in the almost all area, the temperature structure is different from that observed with the CTD at site A, and therefore the scenario proposed in 3.1 is not necessarily applicable for wider area. However, if some instabilities would induce the wave breaking, the spectral form could also be like the turbulence of inertial subrange.

In order to estimate the horizontal and vertical distributions of mixing patches, we examine spectrum slopes that are obtained by the dynamic spectrum method as a function of depth and distance. The bands of wavelength used in the least square fitting are smaller than scale of observed internal wave rolls ($\lambda\sim10$ m). The shaded area in Fig. 8a indicates the area with the slope from $-1.70$ to $-1.60$. If we regard the shaded area is turbulent, the left lower thin layer seen in the left lower side has a horizontal scale of 300 m and a vertical scale about 2~3 m. In the upper part, there is another thinner shaded

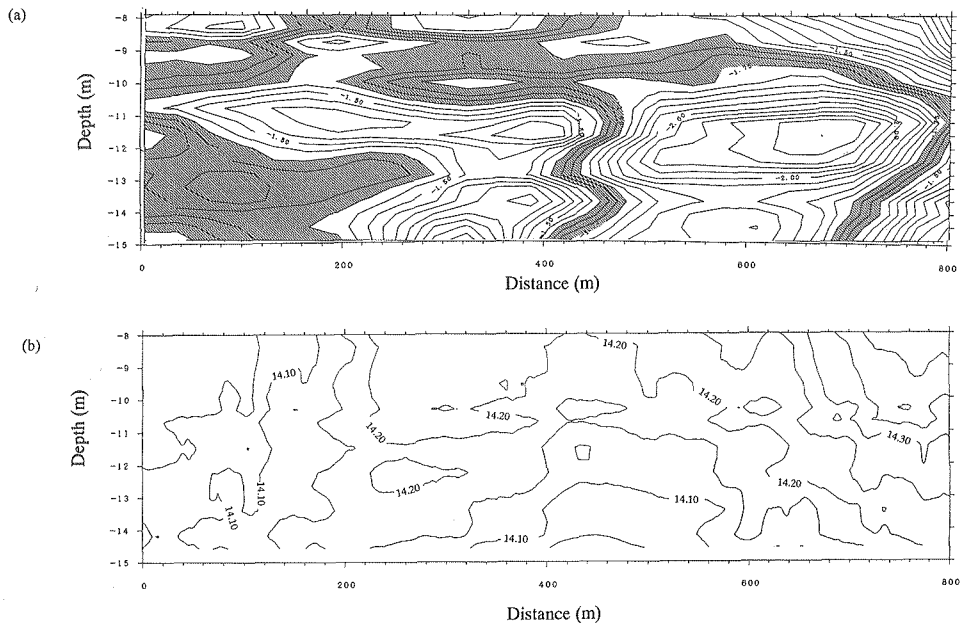


Fig. 8. (a) Distribution of the spectral slopes, and (b) corresponding temperature distribution. The spectral slopes are calculated by a dynamic spectrum method using a horizontally moving window of 512 data points, evaluated at every 100 data point steps. For (a), the contour intervals are 0.05, and regions between −1.60 and −1.75 are shaded. The lower left shaded part in (a) contains the region where breakers were observed, and is likely to be in the inertial subrange. The shaded area in the upper center also indicates the slopes of near −5/3. Although roll like features were not observed in this region, structures that may be associated with convection are detected. So, this area might also be turbulent, though the source of the turbulence might not arise from wave instability.

layer of a vertical size of 1 m. The horizontal scale of this patch is about 200 m.

Comparing the patch distribution to the temperature section shown in Fig. 8b, it can be seen that the lower left part (heavily shaded) presumably corresponds to the turbulence of inertial subrange, which include a isotherm region of about 14.20°C with horizontal extent of about 80 m. When we regard the isotherm of 14.15°C as the right end of the patch, its horizontal scale is about 200 m, while vertical scale is about 1.5 m. The upper thin layer also includes the wide region of isotherm and is bounded by the isotherm of 14.20°C. Consequently, these two thin patches are likely to be produced by mixing. In particular, the left lower layer is almost in the same depth as the internal wave rolls.

### 3.3 *Balance in the TKE equation*

According to Osborn (1980), the eddy coefficient $K_v$, which represents the diapycnal mixing rate of scalar, can be evaluated from the major balance of three terms in turbulent kinetic energy equation. The volume averaged TKE equation for a stratified shear flow (Tennekes and Lumeley, 1972) is given by

$$\frac{\partial}{\partial t}\langle u_i' u_j' \rangle = -\langle u_i' u_j' \rangle \frac{\partial \boldsymbol{U}_i}{\partial x_j} - \varepsilon - \frac{g}{\rho}\langle w' \rho' \rangle + \left\langle \rho' \frac{\partial}{\partial x_j} u_j' p' \right\rangle + \frac{\partial}{\partial x_j}\left[ \nu \langle u_j' \sigma_{ij} \rangle - \frac{1}{\rho}\langle u_j' p' \rangle - \boldsymbol{U}_j \langle u_i' u_j' \rangle \right] \tag{1}$$

where $x$ is the distance, $u$ the velocity, $w$ the vertical velocity. Suffix $i$ and $j$ indicate the two orthogonal components in the three-dimensional space, $p$ the pressure, $\rho$ the density, $g$ the acceleration due to the gravity, primes indicate the variables for perturbation field, $\boldsymbol{U}$ is the mean velocity, and dissipation rate, $\varepsilon$, is given as follows,

$$\sigma_{ij} = \frac{\partial u_i'}{\partial x_j} + \frac{\partial u_j'}{\partial x_i} \quad \text{and} \quad \varepsilon = \frac{1}{2} c \sqrt{\langle \sigma_{ij} \sigma_{ij} \rangle} \tag{2}$$

Usually, (1) is approximated by the following equation.

$$\overline{u'w'} \frac{\partial \bar{U}}{\partial z} + \frac{g}{\rho} \overline{\rho' w'} + \varepsilon = 0 \tag{3}$$

where $u$ is the horizontal velocity and $z$ is the vertical distance. In (3), the 'pressure-velocity correlation' term $\langle w'p' \rangle$ in (1) is usually neglected because $\langle w'p' \rangle$ has been considered not to be important for an isolated turbulent patch in the thermocline. However, the validity to neglect the 'pressure-velocity correlation' term is not clear. In this subsection, we address this question.

For the direct estimation of the amplitude of this term, we must know dissipation rate of the turbulence in the microstructures. Therefore, we estimate the uppermost value of this term without microstructure information as described below.

In order to investigate the relative importance of energy flux by internal waves, a simple model schematized as Fig. 9, following, Wijesekera et al. (1993). It is noted that following argument is for the region containing the internal wave rolls. Within the stratified fluid, there exists a turbulent region, and ambient shear of simple form. Traveling pressure perturbation generates lee waves, which have phase velocities equal to the velocity at the patch boundary (determined by the mean shear, $2\Delta U/L_p$). It is assumed that wave energy is radiated

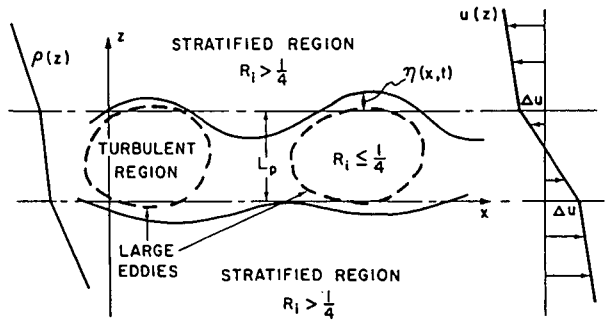


Fig. 9. Schematic representations of internal waves generation from a turbulent patch. Traveling pressure perturbations in the presence of mean shear (e.g., generation of lee waves). The phase velocity of the generated waves are assumed to be equal to the velocity at the patch boundary (determined by the mean shear of $2\,\Delta U/L_p$) [from Wijesekera et al., 1993].

from top and bottom horizontal layers owing to traveling pressure perturbations as shown in Fig. 9. For simplicity, the patch is assumed to be marginally stable to shear instabilities; that is, $R_i \approx 0.25$, whereas fluid outside the patch has $R_i > 0.25$. The vertical size of a mixing patch $L_p$ is generally proportional to the characteristic turbulent length scales such as the Ozmidov scale. It is therefore assumed that the perturbations at the patch boundary are highly correlated with the variability of the Ozmidov scale $L_o$, which is mainly controlled by $\varepsilon$. Consider a two dimensional $(x, z)$ sinusoidal disturbance $\eta(x, z, t)$ at the patch boundary as shown in Fig. 9, where $\eta$ is specified as

$$\eta(x, z, t) = \eta_0 \exp\left[-i(kx + mz - \omega t)\right] \tag{4}$$

with

$$\eta_0 = \zeta L_o = \zeta \sqrt{\frac{\varepsilon}{N^3}} \tag{5}$$

where $t$ is the time, $k$ is the horizontal wavenumber, $m$ is the vertical wavenumber. $L_o$ is the Ozmidov scale ($\equiv(\varepsilon/N^3)^{1/2}$), $\zeta$ is the deviation of $L_o$ as a result of the variability of the $\varepsilon$ (Wijesekera et al., 1993).

Assuming that generated waves travel at the velocity of the interface, the phase speed $c$ of a traveling disturbance can be approximated to $c = \Delta U$. The magnitude of $\Delta U$ is obtained by keeping the patch averaged Richardson number $Ri$ at 0.25, where

$$Ri = N^2/(2\Delta U/L_p)^2 \tag{6}$$

where $L_p$ is the patch height. Then $c$ becomes

$$c=NL_p \tag{7}$$

The wave frequency is simply given by $\omega=ck$. The wave energy flux radiation from both top and bottom layer of the patch is [see Gill, 1982, chapter 6]

$$F_z=\overline{p'w'}=Ew_g \tag{8}$$

where $F_z$ is the energy density, and $w_g$ is the vertical group velocity. The overbar denotes an average over phase. Using the property of linear waves, (8) can be reduced to

$$\overline{p'w'}=2\left[\frac{1}{2}\,c\,\eta_0^2N^2\left(\frac{\omega}{N}\right)^2\left[\left(\frac{N}{\omega}\right)^2-1\right]^{\frac{1}{2}}\right] \tag{9}$$

The vertical divergence of the energy flux is evaluated as

$$\frac{\partial}{\partial z}\overline{p'w'}\cong\frac{\overline{p'w'}}{L_p} \tag{10}$$

The upper bound of $(\omega/N)^2\,[(N/\omega)^2-1]^{\frac{1}{2}}$ is $1/2$ ; therefore, by substituting (5), (7) and (9) to (10), it is shown that the divergence of energy flux satisfies

$$\frac{\partial}{\partial z}\overline{p'w'}\leq\frac{1}{2}\,\zeta^2\varepsilon \tag{11}$$

Here, the upper bound of $\partial/\partial z(\overline{p'w'})$ relative to $\varepsilon$ depends only on $\zeta$, the ratio of amplitude $\eta$ to the Ozmidov scale $L_o$.

The Ozmidov scale is usually determined from the distribution of the dissipation rate, which is not known in the present study. However, according to the comparison of the Ozmidov scale $L_o$ and the Thorpe scale $L_t$ for the CEAREX data, it is known that $L_o/\,L_t$ is nearly unity for usual eddies (Wijeserkera et al. 1993). Thorpe scale represents the largest vertical scale of possible overturning events. Therefore, $L_t$ is used to estimate the $\partial/\partial z(\overline{p'w'})$, instead of $L_o$ in (5). For the calculation of the Thorpe scale, we need density distribution, though the TSP observes only the temperature. Therefore, we must estimate the salinity distribution from the temperature using a T-S relation. Although the salinity does not have unique relation to the temperature as shown in Fig. 4, with a temperature minimum at 14 m depth. We used the T-S relation shallower than 14 m depth, since the wave rolls and mixing patches locate in the depth shallower than 14 m. In shallower depths than the depth of the TSP observation, we assumed that the density is uniform. Also, deeper than 22 m, temperature is assumed to increase linearly to 14.7°C of bottom boundary layer. Resultant density profiles are modeled as shown in Fig. 10, which indicate the

estimated density profile at a distance of 18 m from the point where the first internal wave roll is observed.

Figure 11 shows the example of Thorpe displacement corresponding to the density profile shown in Fig. 10. For a given profile of the Thorpe displacement, $d_i$, the Thorpe scale is defined by rms value of them (De Silva and Fernando, 1992), as

$$L_t=\left[\frac{1}{n}\sum_{i=1}^{n}d_i^2\right]^{\frac{1}{2}}. \tag{12}$$

Estimated $L_t$ are shown in Fig. 12 as a function of the distance from the point

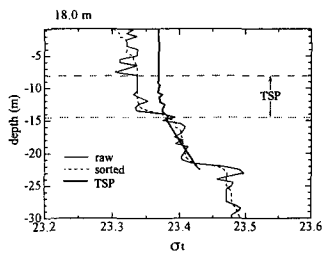


Fig. 10. Density profile estimated from a temperature profile observed with TSP (solid line). The thin line indicates the density from CTD at site A, and dashed line is the Thorpe-ordered density, both of which were also shown in Fig. 4. The vertical extent of the TSP observation as denoted by "TSP". The density above this region is estimated as uniform, and the density below this region is assumed to increase linearly (see also text). The density profile is at a distance of 18 m from the point where the first internal wave roll is observed.

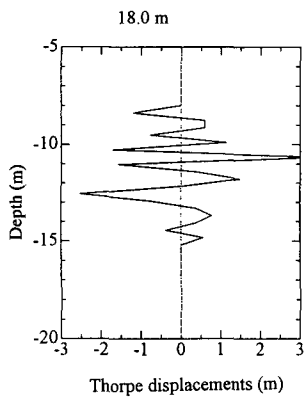


Fig. 11. Profile of Thorpe displacements *di* corresponding to the density profile shown in Fig. 10.

where the first internal wave roll is observed, and are ranging from 1. 14 m-1.60 m.

In order to examine the disturbance of the patch boundary, we estimated the mean temperature $\bar{T}$ at each depth. Then the mean vertical gradient $\bar{T}_z$ was estimated as a function of $z$. Obtained $\bar{T}_z$ is ranging from $-0.04°Cm^{-1}$ to $0.04°Cm^{-1}$. $\bar{T}_z$ of absolute value less than $0.01°Cm^{-1}$, were corrected to $0.015°Cm^{-1}$, the least temperature gradient that the TSP can resolve. Now, for a selected depth, an instantaneous temperature $T(t)$ can be related with the vertical displacement $\eta$ as follows

$$T(t)=\bar{T}+\bar{T}_z\eta. \tag{13}$$

We can estimate $\eta$ by solving (13) as,

$$\eta=\frac{T(t)-\bar{T}}{\bar{T}_z} \tag{14}$$

Figure 13 shows the vertical displacement given by (14) for the corresponding sensor depth. The variation of temperature in Fig. 13 is often spiky. In order to know the wavelength of dominant amplitude waves, Fourier decomposition was applied to the temperature time series. The structure for the depth where the internal wave rolls were observed has a dominant peak at a wavelength of 15 m (Fig. 14(a)), but there is no such remarkable peak out of the depths of the rolls (Fig. 14(b)). This wavelength 15 m of dominant amplitude, is exactly the

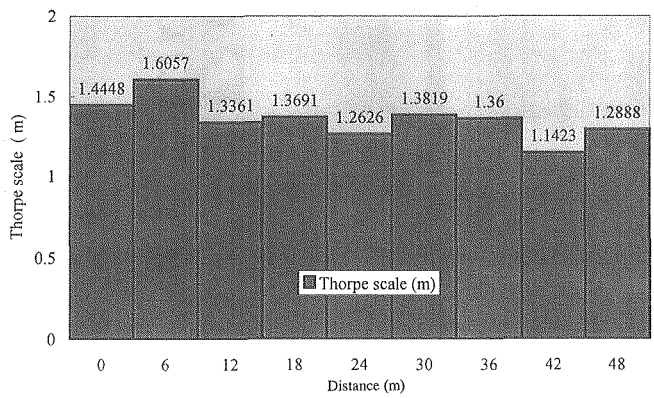


Fig. 12. Thorpe scale as a function of the distance from the point where the first internal wave roll is observed. The Thorpe scales are ranging from 1.14 m to 1.60 m, and hence the difference is the order of 0.5 m. The difference is comparable with the Fourier amplitude of the isotherm displacement at a 15 m wavelength (see also Fig. 13.).

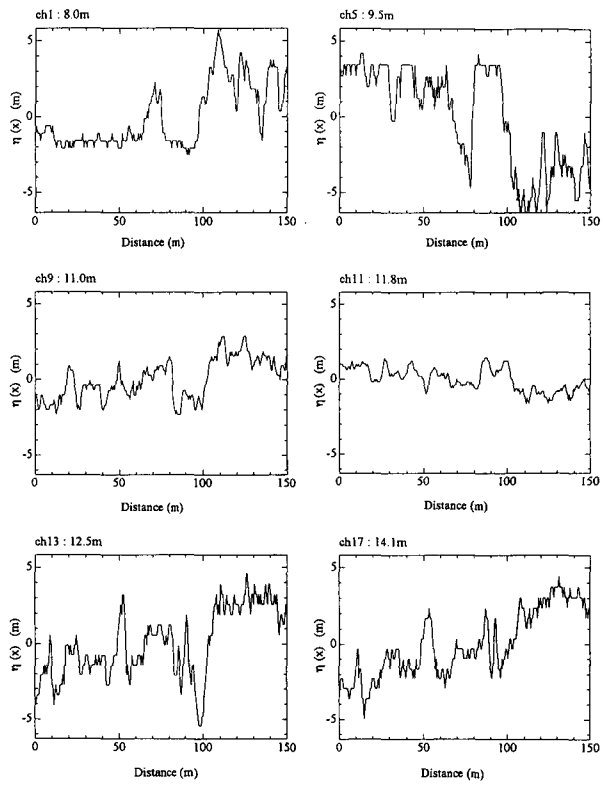


Fig. 13. The vertical displacements of isotherms for some sensor depth. Calculation are for the 150 m width region, which include the alignment of breakers.

same scale of observed internal wave rolls. For the case of shear instability, mixing patches are expected to remain the features of the organized wave trains before spreading to pancakes. So the patch boundary should have about the same wavelength as the occurrence of the breaking waves (see also Fig. 9.17 of Munk, 1981). Thus, for the region considered here, it can be concluded that the waves of 15 m wavelength broke, and left the patches whose surface is characterized by the perturbations of the same 15 m wavelength.

Figure 14(a) shows that $\eta$ of 15 m wavelength is ranging from 0.3 m to 1.0 m, whereas $L_t$ is from 1.1 m to 1.6 m. Thus, $\zeta$ $(=\eta/L_t)$ takes the value from 0.19 to 0.91. When $\zeta$ is 0.19, the relative magnitude of the 'divergence of pressure-velocity correlation' to dissipation rate $\varepsilon$ is less than 2%. In this case, as Wijesekera et al. (1993) concluded, omission of the divergence term is valid. On the contrary, taking the value of $\zeta$ as 0.91, the magnitude of the divergence term

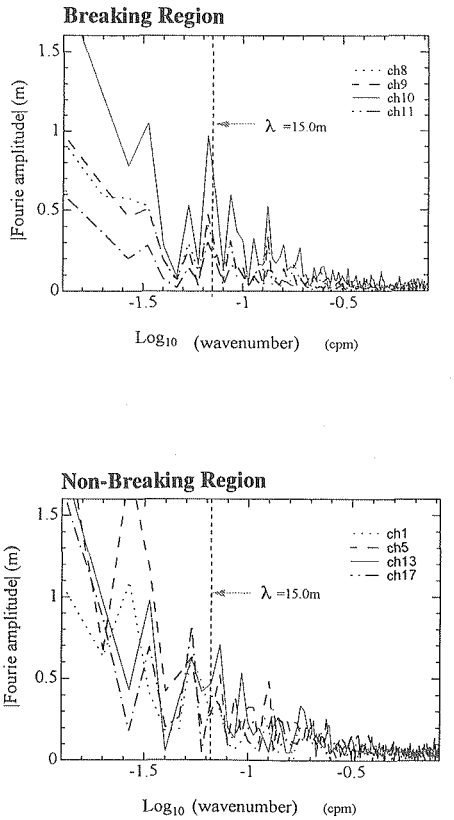


Fig. 14. Fourier amplitudes of isotherms' displacements $\eta$. It span the horizontal scale 1 m to 150 m. The amplitudes for the depth where breakers were observed are shown in (a), and those out of the breaker depths are shown in (b). The amplitudes commonly have peaks at a 15 m wavelegth for the breaker depth. Nevertheless no such features are seen outside this depth range.

relative to the dissipation rate can rise as high as 40%.

Let $C_{cd}$ denote the $p$-$v$ correlation divergence, the TKE equation (3) becomes

$$P=B+\varepsilon-C_{cd} \tag{15}$$

where $P$ is the shear production rate, and $B$ is the buoyancy flux. In a case of no $C_{cd}$ term, the kinetic energy produced by shear transformed partly to potential and the remainder is dissipated. However, in the case where the $C_{cd}$ term cannot be neglected, a part of energy is redistributed through fluctuation

of pressure and velocity. As the result, the rate of dissipation is slightly reduced.

The relation (15) can be rewritten as

$$P=B+\varepsilon_0 \tag{16}$$

where

$$\varepsilon_0=\varepsilon\left(1-\frac{C_{cd}}{\varepsilon}\right). \tag{17}$$

Obviously, $\varepsilon_0$ represents the true dissipation rate in the case of no omission of the $p$-$v$ correlation divergence term.

From the equation (16), we can derive the turbulent diffusion coefficients, $K_{\rho_0}$, as

$$\begin{aligned} K_{\rho_0}&=\frac{R_f}{1-R_f}\frac{\varepsilon}{N^2} \\ &=K_\rho\left(1-\frac{C_{cd}}{\varepsilon}\right) \end{aligned} \tag{18}$$

In the present estimate, the higher value of the ratio of the $p$-$v$ correlation divergence term to the kinetic energy dissipation rate is 0.4, then (18) becomes

$$K_{\rho_0}=0.6\,K_\rho \tag{19}$$

The result shows the possibility that usual estimate of the turbulent diffusion coefficients in the region of internal wave rolls could be overestimated by about 60%, due to omission of energy redistribution term of $C_{cd}$. In that extreme case, the energy flux due to internal waves must not be neglected. From the present results, we cannot conclude whether it is appropriate to neglect the divergence term. Further observational studies are necessary to clarify this uncertainty.

## 4. Summary and Conclusion

A towed temperature profiling system the TSP enable us to investigate the structure of two dimensional vertical temperature section with a high resolution. The observation with the TSP gave us a clear image of internal wave rolls, which have seldom observed so far in the real ocean. Comparing with the pioneering work of Woods (1968), the data obtained by the TSP has advantages because the temperature data obtained by the TSP is suitable for quantitative analyses, such as a spectrum analysis. The major results of the present study are summarized as follows.

1. The observed internal wave rolls (or breakers) have horizontal wavelength of 15 m, and the waveheight of 2 m. According to the stability boundary presented by Thorpe (1978), the internal waves with a wave slope greater than 0.34 should break despite of the condition of ambient shear, and contribute the local mixing. In addition, the required velocity difference for the generation of waves due to shear instability is only about 0.07 $ms^{-1}$ between upper and lower layers. Therefore, we speculated that the TSP has captured the wave rolls that had grown due to the shear instability, just before their breaking.

2. From the slopes of temperature wavenumber spectra, the sizes of mixing patches were estimated. The region of wavenumber dependence near $-5/3$ corresponds to the inertial subrange. The estimated sizes of mixing patches are about 200 m in horizontal, and 2.5 m in vertical, respectively. The low aspect ratio of mixing patches seems to reflect a typical property of stratified turbulence.

3. The validity of neglection of the term of 'divergence of pressure-velocity correlation' in the TKE equation was examined. In order to consider the effect of the energy flux radiation from mixing patches, a simple model of lee wave generated at the patch boundary was applied. From the temperature data with the TSP, vertical displacement and the Thorpe scale were estimated. Applying these length scales to the divergence of pressure-velocity correlation, the upper bound of the divergence term is in the range of 2% and 40% of dissipation rate, $\varepsilon$. In the latter case, this term cannot be ignored.

Although the data of background stratification and shear are too sparse to discuss about the detail of the wave breaking mechanism in the present work, the capturing the internal wave rolls in the form of high resolution digital data supports the effectiveness of TSP in the investigation of internal wave breaking and mixing processes. There are many locations where K-H instabilities may occur frequently. For example, warm core ring's near inertial critical layer where near inertial waves are trapped and should cause shear instability, was explored by Kunze et al. (1995). At the base of mixed layer, also instability might occur. Co-operating with microstructure measurements for direct signals of active mixing events and concurrent velocity measurements to provide the information about the background flow field, TSP will give insights for solving the problem on the link of internal wave breaking and mixing.

## Acknowledgments

We thank Mr. H. Togawa, the President of the Allec Electric Co., and his

staffs for cooperation in the temperature data collections. This study was financially supported by the Ministry of Education, Sciences, Sports and Culture of Japan through the International Cooperative Research Program for Global Ocean Observing System (GOOS).

## References

Desaubies,Y.J.F., and M.C. Gregg, 1981. Reversible and irreversible finestructure. J. Phys. Oceanogr., **11**, 541-556.

Desaubies, Y., and W.K. Smith, 1982. Statistics of Richardson number and instability in oceanic internal waves. J. Phys. Oceanogr., **12**, 1245-1259.

De Silva, I.P., and H.J.S. Fernand, 1992. Some aspect of mixing in a stratified turbulent patch. J. Fluid. Mech., **240**, 601-625.

Eriksen, C.C., 1985. Implications of ocean bottom reflection for internal wave spectra and mixing. J. Phys. Oceanogr., **15**, 1145-1156.

Gargett, A.E., and T.R. Osborn, 1981. Small-scale shear measurements during the Fine and Microstructure Experiment (Fame). J. Geophys. Res., **86**, 1929-1944.

Garrett, C.J.R., 1979. Mixing in the ocean interior. Dyn. Atmos. Oceans, **3**, 239-265.

Garrett, C.J.R., and W.H. Munk, 1979. Internal waves in the ocean. Annu. Rev. Fluid Mech, **11**, 339-369.

Gill, A.E., 1982. Atomospher-Ocean Dynamics, Academic Press.

Gregg, M.C., 1977. Variation in the intensity of small-scale mixing in the main thermocline. J. Phys. Oceanogr., **7**, 436-454.

Gregg, M.C., 1987. Diapycnal mixing in the thermocline. A Review. J. Geophys. Res., **92**, 5249-5286.

Hazel, P., 1972. Numerical studies of the stability of inviscid stratified shear flows. J. Fluid Mech., **51**, 39-61.

Kanari, S., Y. Kaya, T. Hibiya, A. Yuzuriha, 1996. A towed temperature structure profiling system with code-scanning method. Gophys. Bull. Hokkaido Univ., **59**, 107-118 (in Japanese with English abstract).

Kolmogoroff, A.N., 1941. The local structure of turbulence in an incompressible viscous fluid for very large Reynolds number. C.R. Acad. Sci. USSR, **30**, 301-305.

Koop, C.G., and F.K. Browand, 1979. Instability and turbulence in a stratified flow with shear. J. Fluid. Mech., **92**, 135-159.

Kunze, E.R., W. Schmitt, and J.M. Toole, 1995. The energy balance in a warm-core ring's near-inertial critical layer. J. Phys. Oceanogr., **25**, 942-957.

Lafond, E.C., 1963. Towed Sea-temperature structure profiler. Marine Science Instrumentation, **2**,53-59.

Marmorino, G.O., and C.L. Trump, 1992. High-wavenumber shear and temperature structure during the Patches experiment. J. Geophys. Res, **97**, 2309-2318.

Mescar, R., and F. Evans, 1977. Distributed instrumentation profiling system. Exposure, **5**(3), 1-7.

Miles, J.W., 1961. The stability of heterogeneous shear flows. J. Fluid. Mech., **10**, 496-508.

Munk, W.H., 1981. Internal waves and small-scale processes. *Evolution of Physical Oceanography, Scientific Serveys in Honor of Henry Stommmel,* B.A. Warren and C. Wunsch. Eds., The MIT Press, 264-269.

Müller, P., and N. Xu, 1992. Scattering of oceanic internal gravity waves off random bottom topography. J. Phys. Oceanogr., **22**, 474-488.

Orlanski, I., and Bryan, 1969. Formation of the thermocline step structure by large amplitude internal gravity waves. J. Geophys. Res., **4**, 6975-6983.

Osborn, T.R., 1980. Estimates of the local rate of vertical diffusion from dissipation measurements. J. Phys. Oceanogr., **10**, 83-89.

Richardson, L.F., 1920. The supply of energy from and to atmospheric eddies. Proc. R. Soc. London, **A97**, 354-373.

Tennekess, H., and J.L. Lumely, 1972. A First course in turbulence. 300 pp., MIT Press, Cambridge, Mass.

Thorpe, S.A., 1973. Turbulence in stably stratified fluids: A review of Laboratory experiments. Boundary-Layer Met., **5**, 105-119.

Thorpe, S.A., 1978. On the shape and breaking of finite amplitude internal gravity waves in a shear flow. J. Fluid. Mech., **85**, 7-31.

Wijesekera, H.W., T.M. Dillon, L. Padman, 1993. Some statistical and dynamical properties of turbulence in the oceanic pycnocline. J. Geophys. Res., **98**, 22665-22679.

Woods, J.D., 1968. Wave-induced shear instability in the summer thermocline. J. Fluid Mech., **32**, 791-800.